JOURNAL OF GEOPHYSICAL RESEARCH, VOL. 90, NO. C6, PAGES 11,689–11,707, NOVEMBER 20, 1985

CO_2-Induced Change in a Coupled Ocean-Atmosphere Model and Its Paleoclimatic Implications

SYUKURO MANABE AND KIRK BRYAN, JR.

Geophysical Fluid Dynamics Laboratory/NOAA, Princeton University, Princeton, New Jersey

The climatic effects of very large changes of CO_2 concentration in the atmosphere are explored using a general circulation model of the coupled ocean-atmosphere system. As a simplification the model has an annual mean insolation and a highly idealized geography. A series of climatic equilibria are obtained for cases with $\frac{1}{2}$, $1/\sqrt{2}$, 1, 2, 4, and 8 times the present CO_2 concentration in the atmosphere. The results from these six numerical experiments indicate the climatic signatures of large CO_2 changes in the atmosphere and in the abyssal and surface waters of the ocean. As the CO_2 concentration in the model atmosphere increased from 1 to 8 times the normal value, the meridional gradient of surface air temperature decreased, while that of upper tropospheric temperature increased in agreement with the results of earlier CO_2 climate sensitivity studies. However, the intensity and latitudinal placement of the atmospheric jet hardly changed. Despite the reduction of meridional temperature gradient, the meridional density gradient of water at the ocean surface changed little because of the increase of thermal expansion coefficient of seawater with increasing temperature. Thus the intensity of thermohaline circulation in the ocean model does not diminish as expected in the range from 1 to 8 times the normal atmospheric CO_2 concentration. As was shown in an earlier study, the CO_2-induced changes in the deep sea follow the change of sea surface temperature in high latitudes and thus are much larger than the globally averaged changes of sea surface temperature. The model predicts that the area mean rates of precipitation, evaporation, and runoff increase with increasing CO_2 concentration in the atmosphere. The latitudes of the arid zone and the high surface pressure belt in the subtropics are almost constant in the entire range of 1–8 times normal CO_2. In general, the climatic signature obtained from the model appears to be consistent with a CO_2 hypothesis for the climatic changes in the Cenozoic with the following exception: the tropical sea surface temperature in the model has a small but significant increase with increasing atmospheric CO_2 concentration, while tropical sea surface temperature as deduced from the isotopic record appears to have no systematic trend during the Tertiary. It is found that the climate corresponding to one-half normal CO_2 is markedly different from the normal and high-CO_2 cases. Sea ice extends to middle latitudes, and the thermohaline circulation in the model ocean loses its intensity and is largely confined to an area between the sea ice margin and the equator. The poleward heat transport by ocean currents is very small in high latitudes, markedly reducing the surface air temperature there. It is suggested that a similar process, which enhances the positive albedo feedback effect of sea ice, played a key role in reducing surface air temperatures over the North Atlantic during the last glacial maximum.

1. INTRODUCTION

At the turn of the century, *Chamberlin* [1899] suggested that large variations in the earth's climate may be partly attributable to changing concentration of CO_2 in the atmosphere. On the basis of an estimate of the CO_2 exchange between the atmosphere and lithosphere, *Budyko and Ronov* [1979] suggested a mechanism for long-term atmospheric CO_2 variations. *Budyko and Efimova* [1981], using existing estimates of climate sensitivity to CO_2, concluded that CO_2 variations could be large enough to account for the climate changes indicated by geologic evidence in the Tertiary. *Berner et al.* [1983] have developed a comprehensive model of carbon cycling in the atmosphere, ocean, and lithosphere. According to their estimates, the atmospheric CO_2 concentration in the Late Cretaceous was many times larger than the present value but decreased during the Tertiary. Concrete evidence of significant natural variations during the Quaternary is provided by cores from the Greenland and Antarctic ice sheets. The chemical analysis of air bubbles trapped in the ice indicates that during the last glacial maximum, atmospheric CO_2 concentration was only $\frac{2}{3}$ of the preindustrial value (see, for example, *Neftel et al.* [1982]).

In the past the changing continent and ocean geometry associated with plate tectonics appeared to provide a reasonable explanation for climate variation. By use of a general circulation model of the atmosphere coupled with an idealized swamp ocean without heat capacity, *Barron and Washington* [1984] investigated the role of geographic variables (i.e., topography and surface albedo) in maintaining the warm climate of the mid-Cretaceous epoch. Although these results demonstrated that paleogeography was a substantial forcing factor, its influence was insufficient to explain the warm climate. Before fully accepting their conclusion, it is obviously desirable to investigate the CO_2 climate issue by use of a coupled ocean-atmosphere model in which the effect of oceanic heat transport is taken into consideration.

Using a coupled ocean-atmosphere model specifically designed to evaluate the sensitivity of climate, this study obtains six climate equilibria which correspond to atmospheric CO_2 concentrations varying by a factor of 16. In contrast to many previous studies of climate sensitivity to CO_2, the model allows a calculation of climatic signatures in the ocean as well as on land. Although the geometry is highly idealized, it is hoped that the model results will be useful for evaluating the CO_2 hypothesis for climate change based upon the geologic evidence from both terrestrial and marine environments. Some of the results of this study have already been described in a paper by *Spelman and Manabe* [1984].

2. MODEL STRUCTURE

The model used for this study is identical to the coupled ocean-atmosphere model which was used by *Bryan et al.*

Paper number 5C0607.

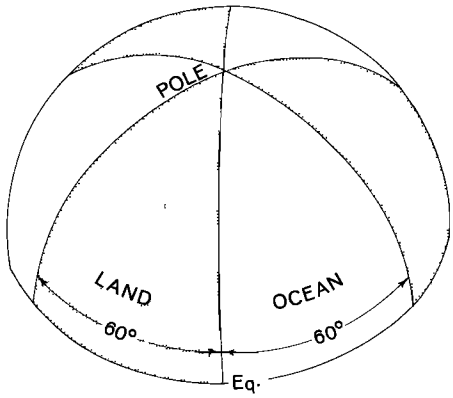

Fig. 1. Idealized geography of the model.

[1982], *Spelman and Manabe* [1984], and *Bryan and Spelman* [this issue] in their studies of transient and equilibrium responses of climate to the change in the atmospheric CO_2 concentration. For computational economy and ease in interpreting the results from numerical experiments, the coupled model has an idealized geography which consists of three identical sets of a pie-shaped continent and ocean shown in Figure 1. In the atmospheric component of the model, cyclic continuity is specified at the meridional boundaries, which are 120° of longitude apart. Thus three identical pie-shaped atmospheres cover the entire hemisphere. A condition of mirror symmetry is imposed at the equator.

In order to illustrate the basic structure of the model, a box diagram is constructed and is shown in Figure 2. According to this figure the model consists of two main components, the general circulation model of the atmosphere and that of the oceans. The atmospheric model predicts the horizontal component of wind vector, surface pressure, temperature, and water vapor content of air based upon the equations of motion, the equation of air mass continuity, the thermodynamical equation, and the prognostic equation of water vapor, respectively. These predictions are conducted by use of the spectral transform method [e.g., *Orszag*, 1970]. The horizontal resolution of the model is determined by the "rhomboidal 15" truncation of spectral components, in which the maximum wave number of zonal waves retained is 15. The version of the spectral model described above was constructed by *Gordon and Stern* [1982].

For the computation of the flux of solar radiation, the annual mean insolation (without diurnal and seasonal variation) is prescribed at the top of the model atmosphere. Referring to *Kondratyev* [1972], the solar constant is assumed to be 1356 W/m^2. The effects of clouds, water vapor, ozone, and carbon dioxide are included in the computation of both solar and terrestrial radiation. The mixing ratio of carbon dioxide is assumed to be constant everywhere. For ozone a zonally uniform, annually averaged distribution is specified as a function of latitude and height. Referring to *London* [1957], cloud cover is also prescribed at zonally uniform values depending upon latitude and height (see Table 1 of *Manabe* [1969] for the cloud distribution used here). The distribution of water vapor is determined from the time integration of the prognostic equation of water vapor.

Precipitation is predicted whenever supersaturation occurs in the model. Precipitation is ordinarily rain, but if the air temperature just above the surface is below freezing, snowfall is forecast. An adjustment scheme is used to represent the moist convection process. Further details of the prognostic system for water vapor are found in the work of *Manabe et al.* [1965].

Surface temperatures of the continent are calculated from the boundary condition of no surface heat storage. This condition implies that the contributions from net fluxes of solar and terrestrial radiation and turbulent fluxes of sensible and latent heat must balance locally. The computation of net solar radiation at the surface requires the specification of surface albedo. The albedo of snow-free continental surfaces is assumed to be zonally uniform and is fixed as a function of latitude as given by *Manabe* [1969]. Over a snow-covered region a larger value of surface albedo is assigned. When the surface air temperature is below −10°C, the albedo is 70%; above −10°C, it is 60%. A change in snow depth is predicted as the net contribution from snowfall, sublimation, and snowmelt, with the latter two determined from the surface heat budget.

The groundwater budget is computed by the "bucket method." The soil is assumed to have a water-holding capacity of 15 cm. If the computed soil moisture exceeds this amount, the excess is assumed to be runoff. Changes in soil moisture are computed from the rates of rainfall, evaporation, snowmelt, and runoff. Evaporation from the soil is determined as a function of soil moisture and potential evaporation rate (i.e., hypothetical evaporation rate from a completely wet soil). Further details of the hydrologic computation can be found in the work of *Manabe* [1969].

The oceanic component of the coupled model is similar to the model described by *Bryan and Lewis* [1979] and *Bryan et al.* [1975] except that the model ocean extends all the way to the pole. Velocity, temperature, and salinity are predicted and density is calculated from an approximate equation of state. In addition, the ocean model includes a simplified method for calculating the growth of sea ice in the polar regions. When sea ice is present, the temperature of the ocean beneath the ice remains at the freezing point, and heat flux through the ice is balanced by the latent heat of freezing or melting at the bottom of the ice. This process, together with the melting of the upper ice surface, sublimation, and snowfall, determines the change of ice thickness. It is assumed that the albedo of sea ice is the same as that of snow cover specified earlier, with the exception of melting sea ice, to which the albedo of 45% is assigned. The computational grid in the ocean model is a latitude-longitude grid having a resolution of 4.4° latitude and 3.8° longitude. Twelve levels in the vertical, as in the work of

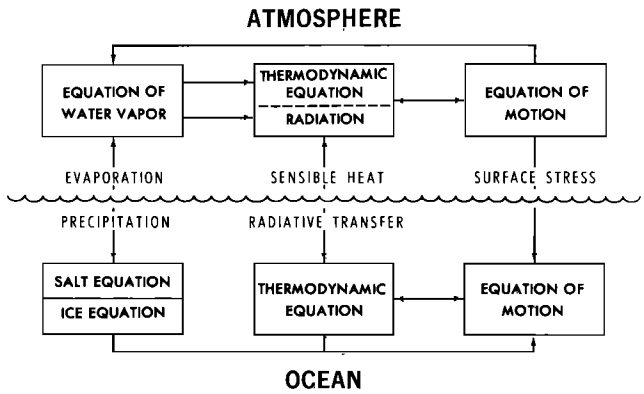

Fig. 2. Box diagram illustrating the major components of the coupled ocean-atmosphere model.

TABLE 1. Placement of the Levels for Vertical Finite Differencing in the Oceanic Component of the Model, and the Coefficients of Vertical and Horizontal Diffusion for Heat and Salinity

Index of Finite Difference Levels	Depth, m	Coefficient of Vertical Diffusion, cm^2/s	Coefficient of Horizontal Diffusion, cm^2/s
1	25	0.30	1.00×10^7
2	85	0.31	0.94×10^7
3	170	0.31	0.87×10^7
4	295	0.31	0.79×10^7
5	483	0.31	0.70×10^7
6	755	0.31	0.62×10^7
7	1131	0.32	0.55×10^7
8	1622	0.33	0.52×10^7
9	2228	0.39	0.51×10^7
10	2935	0.89	0.50×10^7
11	3721	1.24	0.50×10^7
12	4566	1.28	0.50×10^7

The coefficients of vertical and horizontal viscosity have globally uniform values of 20. and 2.5×10^9 cm^2/s, respectively.

Bryan and Lewis [1979], resolve the vertical structure of the ocean to a uniform depth of 5000 m and give a detailed representation of the ocean thermocline. The placement of the finite difference levels and the coefficients of vertical and horizontal subgrid scale diffusion at each level are given in Table 1.

The box diagram in Figure 2 illustrates the interaction among major components of the coupled model. The atmospheric and oceanic components interact with each other through exchanges of heat, water, and momentum. Components of heat exchange are the net radiative flux and turbulent fluxes of sensible and latent heat. The components of water (or ice) exchange are evaporation (or sublimation), rainfall (or snowfall), and runoff (or glacial flow) from the continents. When the water equivalent of accumulated snow exceeds 20 cm, the excess snow is assumed to run off by glacial flow into the ocean. The rate of runoff into the model ocean is computed by assuming that the continental divide is a meridian located at the center of the model continent and that water always flows in the zonal direction. The ocean surface temperature and sea ice are used as the lower boundary condition for the atmosphere. Details of heat, moisture, and the momentum exchange process are given by *Manabe et al.* [1975].

3. Design of Numerical Experiments

In order to evaluate the climatic effects of a large change in the CO_2 concentration of the atmosphere, a series of numerical experiments are conducted by use of the coupled ocean-atmosphere model described in the preceding section. These numerical experiments consist of six long-term integrations of the coupled model with six concentrations of atmospheric carbon dioxide, i.e., 150, 212, 300, 600, 1200, and 2400 ppm by volume. (Hereinafter, these six experiments will be identified as X/2, $X/\sqrt{2}$, 1X, 2X, 4X, and 8X.) The $X/\sqrt{2}$ experiment is added to the original set of five in order to fill the large gap between the results of the 1X and X/2 experiments. The quasi-equilibrium states which emerge from these time integrations are compared with each other to investigate the equilibrium response of the coupled system to a large alteration of the CO_2 concentration in the atmosphere.

An equilibrium state of the ocean-atmosphere model is sought by use of an interactive method which has been successful in previous studies [*Manabe and Bryan*, 1969; *Manabe et al.*, 1975; *Bryan et al.*, 1975; *Bryan*, 1984]. Since the ocean has a much larger thermal inertia (heat capacity) than the atmosphere, the ocean is integrated with respect to time over 110 years concurrently with 1-year integration of the atmosphere. In the deeper layers of the model ocean, the convergence toward equilibrium is accelerated further by a device which is equivalent to artificially reducing the heat capacity of water, as was described by *Bryan* [1984]. Convergence to climate equilibrium for the normal CO_2 experiment is obtained after integrating the model over the period of 7.7 years for the atmosphere and 850 years for the ocean. With the acceleration technique mentioned above, the effective period of time integration for the deeper ocean is 23,000 years. For the increased CO_2 experiments the corresponding time integration periods for the atmosphere, ocean, and deeper ocean are 11.8 years, 1290 years, and 35,000 years, respectively.

The results from the model experiments presented in the following sections represent the time-averaged states of the ocean-atmosphere models over the final 600 days of the atmosphere model integration and 300 years of the ocean model integration. In an extended numerical integration, the convergence to the climatic equilibrium of the normal CO_2 case was tested in a synchronous coupling of the ocean and atmospheric models. Over a 50-year period of the synchronous time integration, the area mean sea surface temperature appears to have no systematic trend and fluctuates around the value reached by the asynchronous integration described above.

4. Discussion of Results

4.1. *Atmosphere*

The change of the thermal structure of the coupled ocean-atmosphere system brought about by a variation in the atmospheric concentration of CO_2 is shown in Figure 3. This figure contains the latitude-height (or depth) distribution of the difference in zonal mean temperature between the 1X and 8X experiments. (For reference the latitude-height distribution of zonal mean temperature from the 1X experiment is also added to the figure.) The increase of the zonal mean temperature of the model atmosphere in response to the eightfold increase in the concentration of atmospheric CO_2 is particularly pronounced near the earth's surface in high latitudes. In low latitudes, on the other hand, the CO_2-induced warming of the upper model troposphere is larger than the corresponding warming of the lower model troposphere. The relatively large increase in the temperature of the upper model troposphere of low latitudes results from the strong control of lapse rate by moist convection as discussed by *Manabe and Wetherald* [1975]. The moist adiabatic lapse rate decreases with increasing atmospheric temperature, causing the increase of the CO_2-induced warming with increasing altitude.

(In evaluating the CO_2-induced change of climate obtained from the present model, one should note that the computation of radiative transfer in the model does not incorporate the effect of 10-μm band of CO_2. By use of a one-dimensional model of radiative, convective equilibrium, S. Fels and M. Schwarzkopf (private communication, 1985) estimated the magnitude of error due to the neglect of this contribution. Their calculations indicate that the surface warming due to eightfold increase in atmospheric CO_2 may be underestimated by about 15%. Therefore it is desirable to keep this in mind when one evaluates the quantitative aspect of the present results.)

The influence of the atmospheric concentration of CO_2

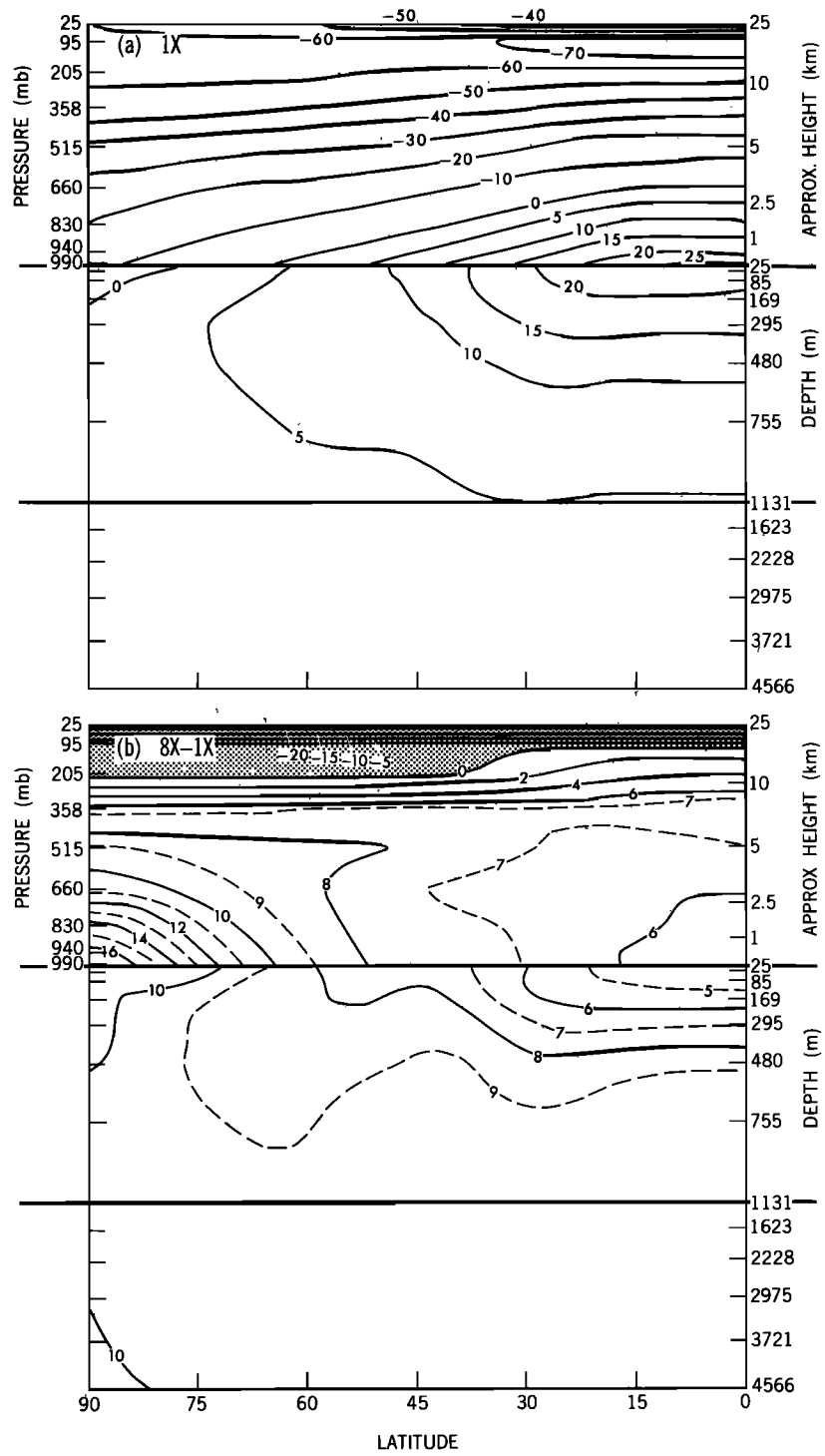

Fig. 3. (*a*) Zonal mean temperature (in degrees Celsius) of the ocean-atmosphere model from the 1X experiment. (*b*) The difference in zonal mean temperature (in degrees Celsius) of the ocean-atmosphere model between the 1X and 8X experiments.

upon the latitudinal profile of surface air temperature is illustrated in Figure 4. The CO_2-induced warming of surface air temperature is particularly pronounced in high latitudes. Thus the meridional gradient of surface air temperature is reduced with increasing CO_2 concentration. The polar amplification described here has been well documented in previous CO_2 climate model studies [e.g., *Manabe*, 1983]. One of the physical mechanisms responsible for this is the poleward retreat of snow cover and sea ice with high surface albedo. Figure 5 illustrates the latitudinal distributions of zonal mean surface albedo from the six experiments. This figure indicates that surface albedo changes markedly as atmospheric CO_2 increases from the X/2 experiment to the 1X experiment owing to the large reduction in the coverage of sea ice and snow. This accounts for the large difference in surface air temperature among the 1X, $X/\sqrt{2}$, and X/2 experiments. Owing to

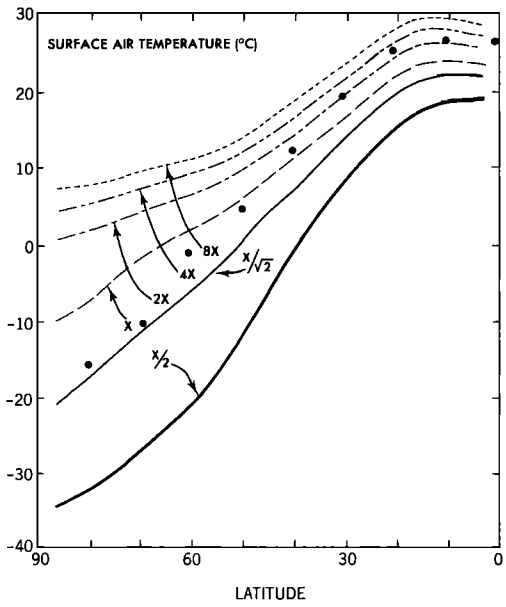

Fig. 4. Zonal mean surface air temperature (in degrees Celsius) of the model atmosphere from the six experiments. Dots indicate the observed values from *Crutcher and Meserve* [1970].

the influence of sea ice upon thermohaline circulation, the poleward heat transport by ocean currents in the X/2 experiment is very small in high latitudes, further reducing the surface air temperature there. Thus the sensitivity of the present coupled atmosphere-ocean model in low-CO_2 experiments is substantially larger than the sensitivity of a model atmosphere coupled to a stagnant ocean mixed layer with comparable surface air temperature as described in the appendix. The positive feedback process involving thermohaline circulation and sea ice will be discussed in detail in section 4.4.

It appears significant that in Figure 4 the difference in surface air temperature between the 4X and 8X experiments increases gradually with increasing latitude despite the very small difference in surface albedo between the two experiments. This result suggests the existence of other mechanisms responsible for this latitudinal dependence of the sensitivity of surface air temperature. Polar amplification in sensitivity is also related to the latitudinal variation of the vertical profile of the CO_2-induced warming in the model troposphere. As Figure 4 indicates, the warming is most pronounced near the earth's surface in high latitudes and reduces sharply with increasing altitude, whereas it is relatively large in the upper model troposphere in low latitudes. Accordingly, the flux of outgoing terrestrial radiation at the top of the model atmosphere in low latitudes increases more per unit increase in surface temperature than the corresponding flux in high latitudes. Therefore the radiative damping of the near-surface temperature anomaly in low latitudes is stronger than the damping in high latitudes and contributes to the increase of the CO_2-induced surface warming with increasing latitude (see *Held* [1978] for further discussion of this topic).

Another mechanism for the polar amplification of the CO_2-induced warming of surface air temperature is the enhanced poleward transport of latent energy in the model atmosphere [*Manabe and Wetherald*, 1980]. For further discussion on this topic, see section 4.4.

As was described in the preceding paragraphs, the meridional temperature gradient in the model atmosphere increases

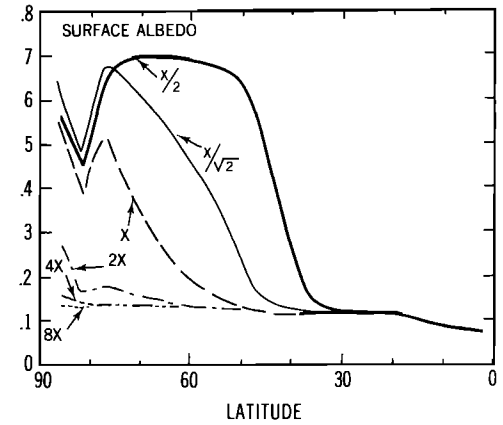

Fig. 5. The latitudinal profiles of zonal mean surface albedo from the six experiments.

with increasing CO_2 concentration near the earth's surface, while the meridional temperature gradient reduces in the upper troposphere. Because of these opposite changes in meridional temperature gradient, the zonal component of total thermal wind shear vector between the earth's surface and the upper troposphere of the model hardly changes from the 1X experiment to the 8X experiment. This compensation effect explains why the intensity and the latitudinal profiles of zonal wind at the 205-mbar level from the 1X, 2X, 4X, and 8X experiments shown in Figure 6 are very similar to one another.

One notes, however, that the latitudinal profile of zonal wind in the X/2 experiment is displaced poleward relative to the profiles from all other experiments. In the numerical experiments recently conducted by I. M. Held (private communication, 1985), a similar poleward shift of zonal wind profile occurred in response to a large reduction of solar constant from the normal value when he used a spectral model with an equatorial boundary and with fixed surface albedos. However, such a shift did not occur in a model without an equatorial boundary. In view of the fact that the model used for the

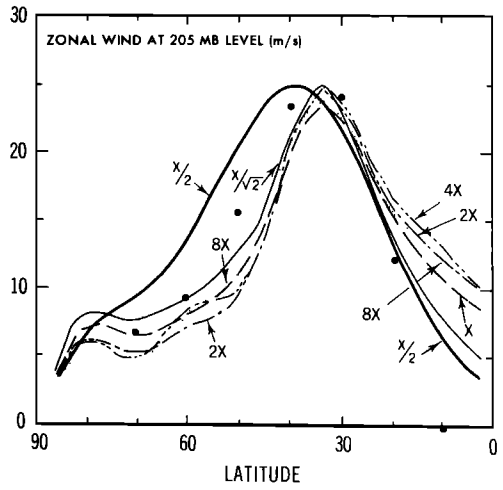

Fig. 6. Latitudinal profiles of zonally averaged, zonal wind (in meters per second) at the 205-mbar level of the model atmosphere from the six experiments. Dots indicate the observed values at the 200-mbar level in the northern hemisphere from *Oort and Rasmusson* [1971].

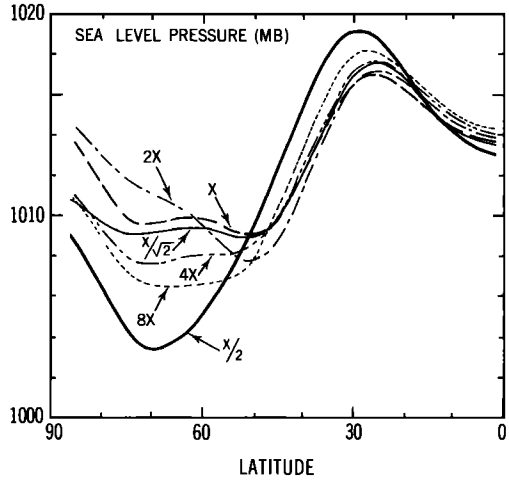

Fig. 7. Latitudinal profiles of zonal mean sea level pressure in the model atmosphere from the six experiments.

present study also has an equatorial boundary, it is possible that the poleward shift of the zonal wind profile from the $X/\sqrt{2}$ to the X/2 experiments may be an artifact of the symmetry condition imposed at the equator.

A similar poleward shift is evident when one compares the latitudinal profile of zonal mean sea level pressure from the X/2 experiment with the profiles from all other experiments shown in Figure 7. Again, in view of Held's experiment, it is possible that this shift is induced by the symmetry constraint. Had we used a coupled model whose computational domain extends over both hemispheres (without the equatorial wall), the subtropical high might very well be located at approximately the same latitude for all (including X/2) experiments.

The latitudinal profiles of zonal mean sea level pressure from the $1/\sqrt{2}$, 1X, 2X, 4X, and 8X experiments are very similar to one another. It is of particular interest that the latitude of the subtropical high hardly changes from the $X/\sqrt{2}$ experiment to the 8X experiment. This constancy of the position of the subtropical high is consistent with the constancy of evaporite deposits in the geological record, which will be discussed later, in section 4.5.

Recently, D. Rind (private communication, 1985) attempted to simulate both a warm Cretaceous climate and a cold ice age climate by use of a general circulation model of the atmosphere with prescribed distribution of sea surface temperature. His results clearly indicate that the latitudinal placements of the jet stream and subtropical high are almost the same in the simulated warm and cold climates.

Despite the lack of sensitivity of zonal wind, the intensity of the Hadley cell changes significantly from one experiment to another. According to Figure 8, which illustrates the streamlines of meridional circulation obtained from both the 1X and 8X experiments, the Hadley cell intensifies in response to the eightfold increase of the CO_2 concentration in the model atmosphere. This intensification is attributable to the increase in the efficiency of moisture supply to the tropics caused by the CO_2-induced enhancement of evaporation in the subtropics. This enhancement in moisture supply results in the increase of

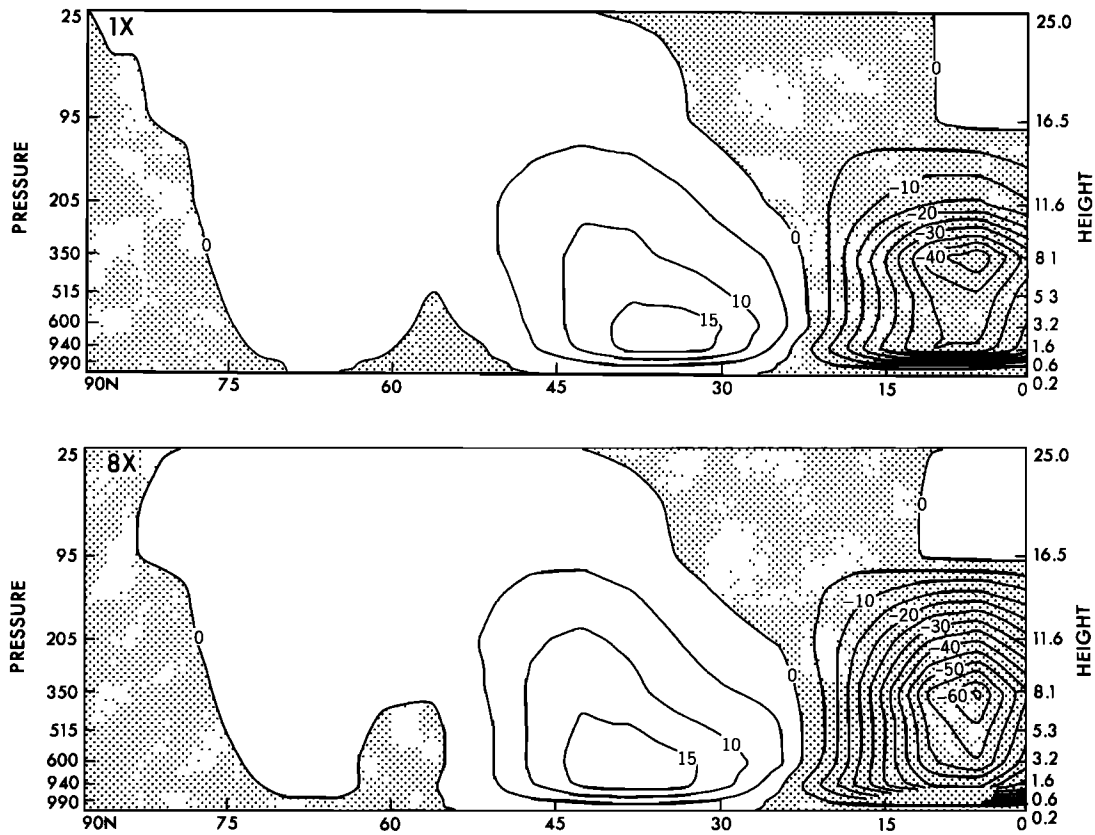

Fig. 8. The latitude-height distributions of the stream function of meridional circulation in the model atmosphere from the 1X (top) and 8X experiments (bottom). Units are in 10^{12} g/s. Note that the meridional mass transport illustrated here represents the transport over three sector atmospheres spanning an entire latitude circle.

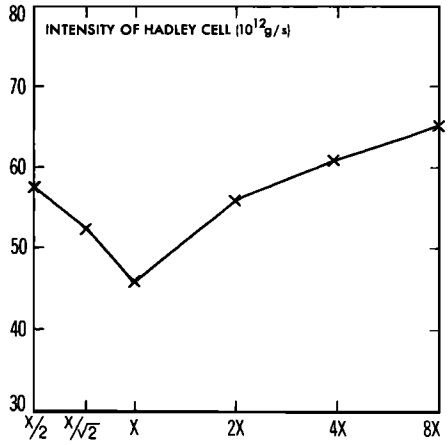

Fig. 9. The intensity of the Hadley circulation in the model atmosphere is plotted for the six experiments. Units are in 10^{12} g/s. Note that the meridional transport illustrated here represents the transport over three sector atmospheres spanning an entire latitude circle.

heat released by condensation and, accordingly, in the intensification of the Hadley cell.

Figure 8 also indicates that the Hadley cell not only intensifies but also becomes taller as the CO_2 concentration increases from the 1X experiment to the 8X experiment. Similar upward stretching of the Hadley cell was noted by *Held and Hoskins* [1985] when they discussed the equilibrium response of the atmospheric model to a 10% increase of solar constant. This stretching is attributable to the intensification, higher penetration of moist convection, and the consequent reduction of vertical temperature gradient in the model tropics.

Figure 9 shows how the intensity of the Hadley cell in the model tropics depends upon the atmospheric CO_2. According to this figure the Hadley cell is weakest in the 1X experiment and intensifies with either increasing or decreasing CO_2 concentration. The large meridional temperature gradient in the lower model troposphere appears to be responsible for the intense Hadley cell in the X/2 experiment. As the temperature of the model troposphere reduces from the 1X experiment to the X/2 experiment, the intensity of the Hadley cell is affected more by the increase in meridional temperature gradient than by the reduction in moisture supply to the tropical rainbelt.

4.2. *Ocean*

One also notes a polar amplification of CO_2-induced change in surface temperature in the model ocean. Figure 10*a* illustrates the latitudinal distributions of zonal mean sea surface temperature (SST) from all six experiments. The CO_2-induced SST change in low latitudes is much smaller than the corresponding change in middle and high latitudes. However, the polar amplification of the SST change is smaller than that of surface air temperature when the concentration of atmospheric CO_2 is low. This is because SST cannot fall below -2°C, the freezing point of seawater. For example, zonal mean SST is almost independent of latitude poleward of 50° in the X/2 experiment. According to Figure 10*b*, sea ice has a zonal mean thickness of approximately 2 m at 50° latitude and becomes thicker with increasing latitude. The absence of meridional gradient in sea surface temperature in high latitudes is partly responsible for the weak thermohaline circulation in the X/2 experiment as described later.

It is of particular interest that the differences of zonal mean temperature in the deep layer of the model ocean between the 8X and 1X experiments is as large as the sea surface temperature difference in high latitudes (see Figure 3). Accordingly, the CO_2-induced warming of the deep model ocean is significantly larger than the area-averaged warming of surface water [*Spelman and Manabe*, 1984]. As will be described later, the relatively cold water in high latitudes sinks and occupies the deep layer of the model ocean in both the 8X and 1X experiments.

As was mentioned in the introduction, *Berner et al.* [1983] estimated the temporal variation of CO_2 concentration in the atmosphere by use of a quantitative model of the carbon cycle. Their results indicate a severalfold reduction in the atmospheric concentration of CO_2 during the Tertiary. Therefore it is worthwhile to compare the distribution of the CO_2-induced change of the oceanic temperature described above with the change of temperature during the Tertiary estimated by use of stable isotope data. Figure 11 shows the temporal variations of isotopic temperatures which are determined from the analysis of planktonic and benthic foraminifera from deep-sea cores [*Savin*, 1977]. The left half of the figure contains the data from deep-sea cores in the North Pacific Basin which occupied a tropical position throughout the Late Cretaceous and the Tertiary. The right half of the figure contains the data from deep-sea cores in the Subantarctic Pacific which were located at high latitudes throughout the Tertiary.

According to Figure 11 the isotopic temperature of the deep ocean has decreased markedly during the last 70 m.y. A reduction of almost the same magnitude also occurred for the sea surface temperature in high latitudes. On the other hand, the isotopic temperature for the planktonic foraminifera in low latitudes shown in Figure 11 appears to have decreased slightly during the same period. In interpreting the isotopic temperature in Figure 11, it should be noted, however, that

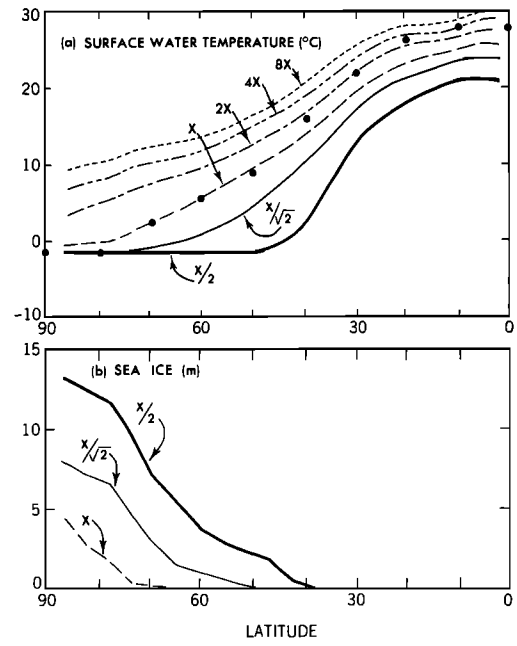

Fig. 10. (*a*) Zonal mean surface water temperature (in degrees Celsius) of the model ocean obtained from the six experiments. Dots indicate the observed values in the northern hemisphere from the *U.S. Navy Hydrographic Office* [1964]. (*b*) Zonal mean thickness of sea ice (in meters) in the model ocean from the 1X, X/$\sqrt{2}$, and X/2 experiments.

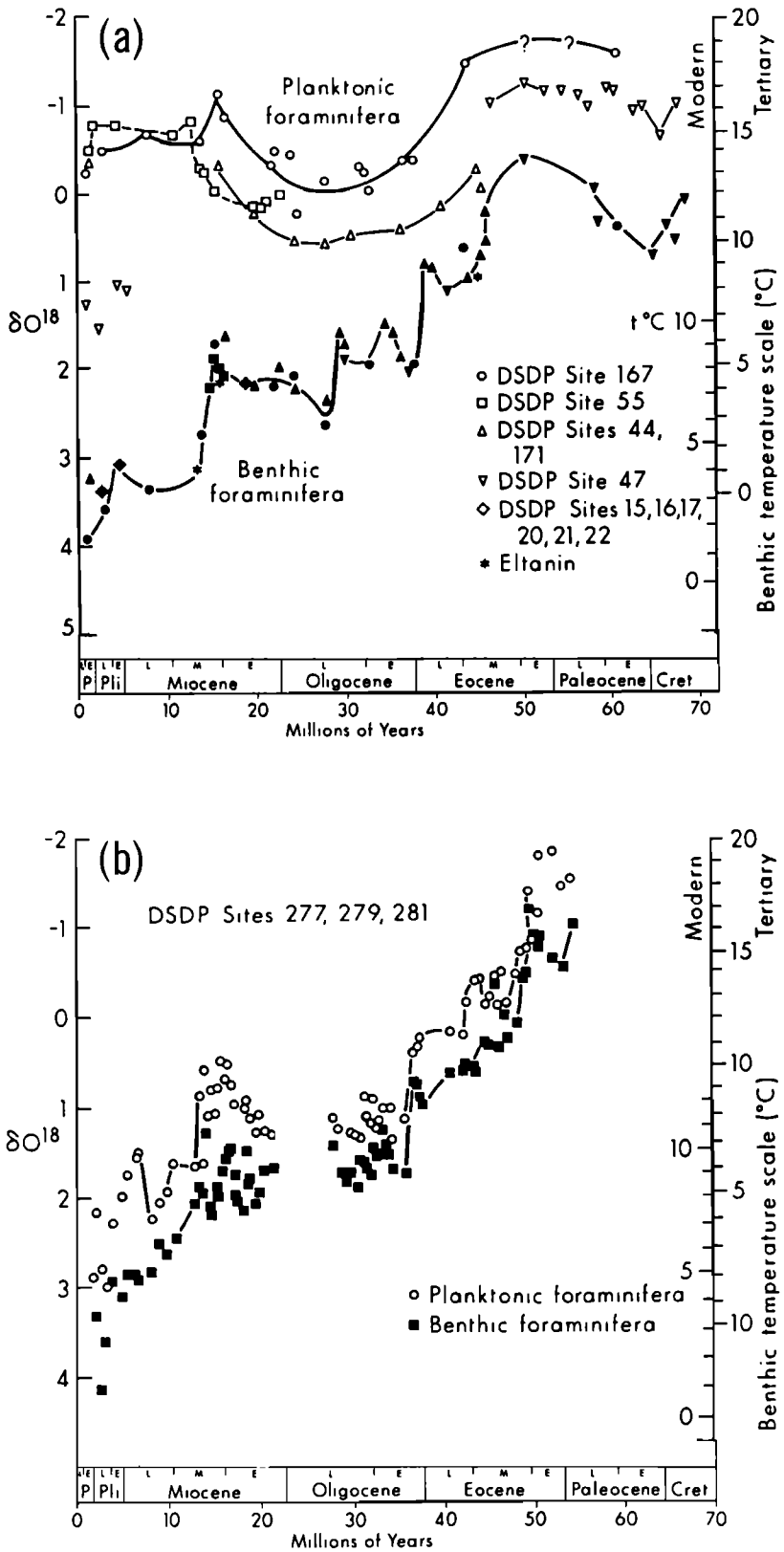

Fig. 11. Isotopic temperature data for Tertiary planktonic foraminifera (open symbols) and benthic foraminifera (solid symbols) compiled by *Savin* [1977]. The modern and Tertiary benthic temperature scales were calculated assuming water $\delta^{18}O$ values of -0.08 and -1.00‰, respectively. (*a*) Data primarily from the North Pacific sites which are believed to have occupied tropical positions throughout the Late Cretaceous and Tertiary. To estimate isotopic temperatures of planktonic foraminifera, add approximately 2.5°C to the appropriate benthic temperature scale. (*b*) Data from the Campbell Plateau and the Macquarie Ridge (Subantarctic Pacific) as analyzed by *Shackleton and Kennett* [1975]. Because of the extreme oceanographic changes in the area during the Tertiary, a separate temperature scale for planktonic foraminifera was not estimated.

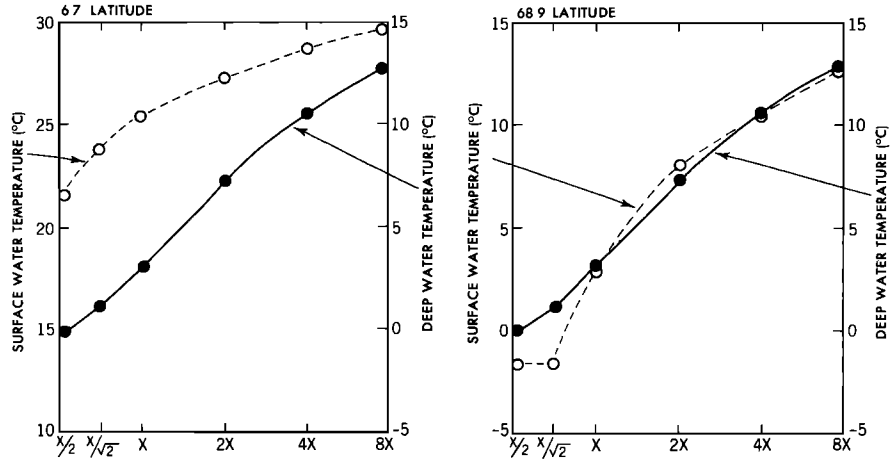

Fig. 12. Zonal mean temperature (in degrees Celsius) of surface water and deep water (depth of 4566 m) at 6.7° latitude (left) and 68.9° latitude (right) of the model ocean from the six experiments.

planktonic foraminifera usually live below sea level. Therefore their isotopic temperature is not necessarily equal to sea surface temperature, particularly in low latitudes where the vertical temperature gradient is large in the upper layer of the oceans. After making some implicit assumptions about the habitation depth of planktonic foraminifera, *Savin et al.* [1975] deduced by extrapolation the sea surface temperature of tropical oceans from isotopic temperatures. Their result indicates no systematic trend during the Tertiary.

In order to compare quantitatively the CO_2-induced change of the temperature of the model ocean with the temporal variation of isotopic temperature shown in Figure 11, Figure 12 is constructed. This figure illustrates the dependence of surface and deep-sea temperatures upon atmospheric CO_2 concentration in both low and high latitudes. According to this figure the oceanic temperature of the model increases in approximate proportion to the logarithm of the CO_2 concentration in the atmosphere. The total difference in temperature between the 1X and 8X experiments amounts to about 10°C both in the sea surface of high latitudes and in the deep sea. This is not very different from the total reductions of the isotopic temperature in both regions during the last 70 million years (see Figure 11).

In low latitudes of the model, the temperature of the deep ocean decreases with decreasing CO_2 concentration in the same manner as in high latitudes. On the other hand, the reduction of sea surface temperature is only 4°C from the 8X experiment to 1X experiment and is much smaller than the corresponding reduction of the deep-sea temperature.

In summary, the general characteristics of Figure 12 described above are very similar to those of Figure 11, provided that the logarithm of atmospheric CO_2 concentration corresponds to time. The similarity between these two figures appears to support the CO_2 hypothesis of Tertiary temperature change. However, one should recall that the surface temperature of the tropical Pacific estimated by Savin et al. has no systematic trend during the Tertiary, although the zonal mean sea surface temperature in low latitudes of the present model has small but significant dependence upon the CO_2 concentration of the atmosphere. In view of the uncertainty involved in their estimate, it may be premature to accept fully their result until it is evaluated by other independent determinations. Nevertheless, the constancy of sea surface temperature in low latitudes is going to be one of the key issues which should be resolved before one can accept the CO_2 hypothesis of the general cooling trend during the Tertiary.

4.3. *Thermohaline Circulation*

The thermohaline circulation of the ocean is very important in the global heat balance. A relatively weak overturning in the vertical meridional plane can be very effective in transporting heat poleward, since there are large vertical gradients of temperature in the ocean and water has such a great heat capacity relative to the atmosphere. Overturning in the meridional plane for the model ocean is shown in Figure 13. The circulation is shown in terms of the transport stream function with the convention that a negative sign indicates counterclockwise circulation. Let us first discuss the reference case for normal atmospheric CO_2. A net sinking is indicated poleward of 60° latitude, and a general rising motion exists equatorward of 60° latitude. Note that the poleward branch of the flow is confined to a shallow surface layer for the most part, while the return flow is rather uniform with depth. This depth profile of the thermohaline circulation makes it particularly effective in transporting heat. Observations by *Bryden and Hall* [1980] and *Roemmich* [1980] indicate that the overturning at 24°N in the Atlantic is approximately 18×10^{12} g/s. Since there is no evidence of bottom water formation in the North Pacific, the overturning measured in the North Atlantic may represent a total overturning for the northern hemisphere. Figure 13 shows that in the normal 1X experiment, the total for the three sector oceans in the hemisphere is about 8×10^{12} g/s at 24°N. Thus the model appears to underestimate the intensity of the thermohaline circulation at this latitude. Recently, *Bryan* [1985] has shown that the intensity of the thermohaline circulation in the models is critically dependent on the vertical mixing coefficient. Without vertical mixing, the surface buoyancy fluxes would not be able to create the large-scale density anomalies that drive the thermohaline circulation. Vertical mixing may be increased to provide an increased driving force for the thermohaline circulation. However, in a low-resolution, viscous model, the thermocline can become unrealistically deep.

As we compare the meridional circulations for different CO_2 climates, it is difficult to determine any significant differences between the reference case and the warm climate cases.

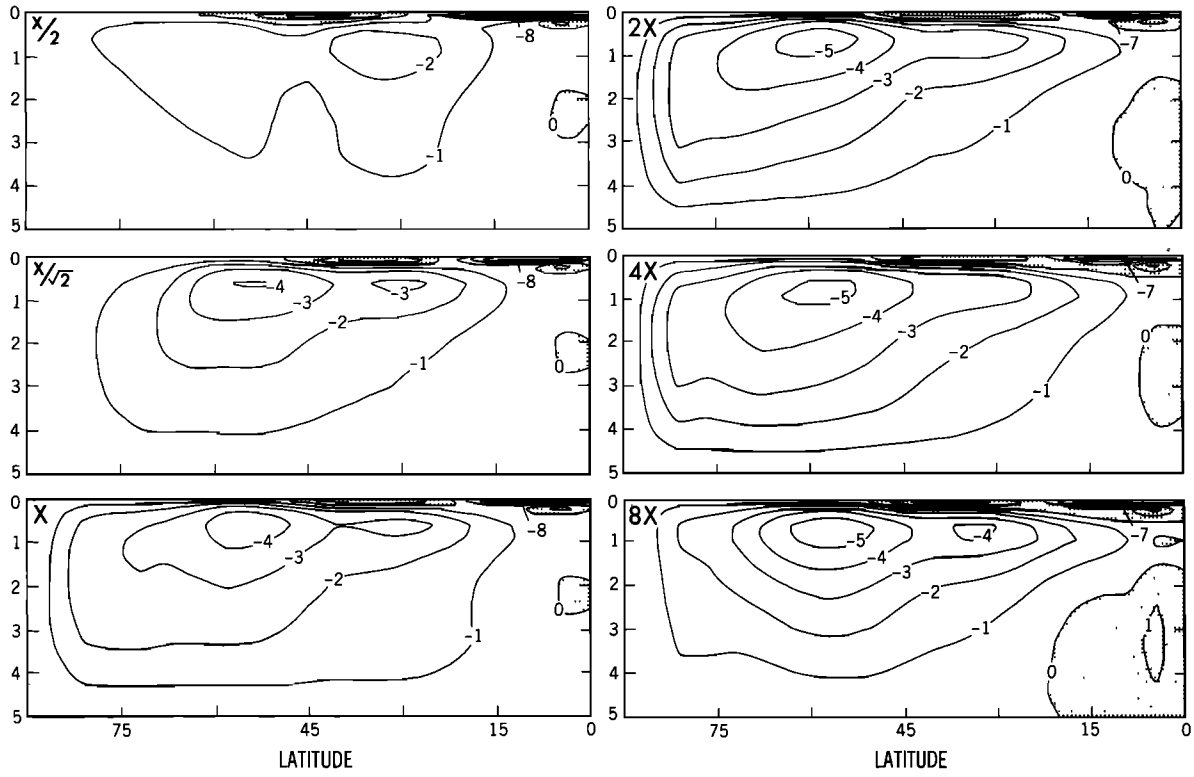

Fig. 13. Streamlines illustrating the meridional circulation in the model ocean from the six experiments. Units are in sverdrups (10^{12} g/s). Note that the meridional mass transport illustrated here represents the transport in one (rather than three) ocean sector.

In all cases the intensity is nearly the same, and there are only minor differences in patterns. The most significant difference exists in the cold X/2 case, where the existence of extensive sea ice has caused a drastic change in ocean circulation. The ice cover confines most of the thermohaline circulation to a smaller range of latitudes between 45° and the equator. The increase in the sea ice coverage suppresses the energy exchange between ocean and atmosphere in high latitudes, weakens the negative buoyancy source, and thus reduces the latitudinal span of thermohaline circulation. The intensity of this smaller meridional cell is only about 50% of that of the larger cell corresponding to warmer climates. In the normal and high-CO_2 climates the thermohaline circulation has a narrow downward branch near the polar wall and a much broader upward branch. In the very cold climate the area covered by sea ice becomes much larger, shifting equatorward the downward branch and its boundary with the upward branches of the thermohaline cell. Thus the area of the upward branch is greatly reduced. Since the vertical advection of heat in the region of upwelling must be balanced by the downward thermal diffusion, the shrinkage of the upward branch implies reduction of total mass flow in the thermohaline cell. As is discussed in section 4.4, the reduction of poleward heat transport due to the weakening of the thermohaline circulation greatly augments the contribution of the albedo feedback process. The combination of these two factors makes the cold climate very sensitive to the decrease of CO_2 concentration in the atmosphere.

From the above discussion it is clear that the intensity of thermohaline circulation depends upon the meridional gradient of density at the ocean surface, which is strongly influenced by heat and water balance of the coupled model. Since the density at the ocean surface is a complex function of temperature and salinity, it is helpful to examine the θ-S diagrams in Figure 14*a*. In Figure 14*a* the dashed curves correspond to zonally averaged temperature and salinities at the ocean surface. A corresponds to the equator, and B, C, D, and E are approximately equal increments of latitude from the equator to the pole. The solid lines in the diagram are a measure of the density in units of sigma-theta, where

$$\text{sigma-theta} = (\rho - 1) \times 10^3 \text{ g/cm}^3$$

and ρ is the equivalent density for a given temperature and salinity referred to surface pressure.

For comparison with the present-day ocean, surface density data from the North Atlantic and North Pacific are compared with the 1X latitudinal profile in Figure 14*b*. The North Pacific is extremely low in salinity, but the model results for normal atmospheric CO_2 (1X) compare very favorably with the North Atlantic data.

Figure 14*a* indicates that all the warm climates (1X, 2X, 4X, and 8X) have similar latitudinal profiles of sigma-theta. Poleward of the equator, temperature decreases but salinity increases with increasing latitudes until a maximum is attained in the subtropics. At higher latitudes, both temperature and salinity decrease with increasing latitude. One can almost reproduce one curve from another by a uniform upward or downward displacement, corresponding to adding a uniform increment of surface temperature at all latitudes. However, a closer examination reveals significant differences. As was noted previously, there is a poleward amplification in the sea surface temperature in response to increased atmospheric

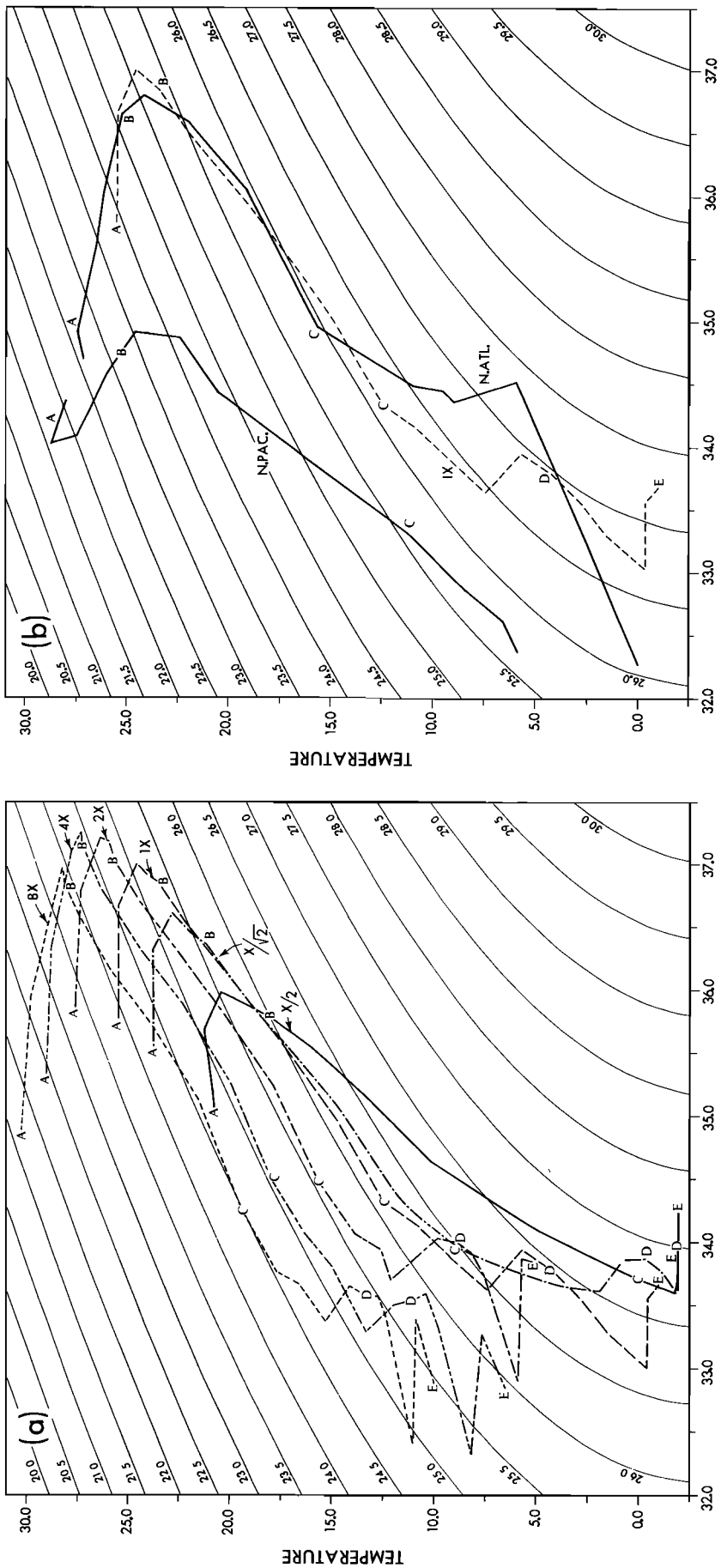

Fig. 14. The temperature-salinity diagrams illustrating the latitude profiles of zonal mean density in units of sigma-theta defined in the main text. (*a*) The profiles of zonal mean density at the depth of 25 m in the model ocean which are obtained from the six experiments. (*b*) The profiles of zonal mean density at the surfaces in the North Atlantic (N. ATL.) and North Pacific oceans (N. PAC.). The density profile from the 1X experiment shown in Figure 14*a* is also shown for comparison. Density is indicated at latitudes of 2.2° (A), 20.0° (B), 42.2° (C), 68.9° (D), and 87.3° (E).

TABLE 2. Difference Between Surface Values of Potential Temperature and of Sigma-Theta at Points A (the Equator) and E (75° Latitude) From Figure 13*a*

Case	$\theta_A - \theta_E$, °C	$\sigma_E - \sigma_A$, 10^{-3} g/cm^3
8X	20.5	4.2
4X	22.5	4.1
2X	22.5	4.1
X	26.0	3.9
X/2	22.5	3.0

With the exception of the X/2 case, temperature contrast with latitude decreases for warmer climates, but the density contrast actually increases slightly.

CO_2. In most cases the change in temperature at point E, the polar point, is much larger than for A, the equatorial point. Note the total ranges of salinity between the subtropics and the equator and between the subtropics and the pole increase slightly with increasing atmospheric CO_2 from the 1X experiment to 8X experiment.

A really significant decrease in the salinity range occurs in the cold X/2 climate. The range is a factor of 2 less than that of the warmest climate. Here again we see the dramatic effect of widespread sea ice cover. The existence of ice also puts a lower limit on temperature at higher latitudes, so that polar surface temperatures cannot be colder, while the tropical temperatures are significantly lower. The total range of temperature is significantly less than that of the 1X climate.

Some of the results shown above are summarized in Table 2. In the first column the total temperature difference between surface waters at the equator and pole is given. A corresponding difference in sigma-theta is shown in the second column. We see that the equator to pole temperature difference decreases as we go to either warmer or colder climates. In the former case, polar amplification is indicated, while the existence of ice is important in the latter case. Intuition would suggest that as the north-south gradient of ocean surface temperature reduces, the gradient of density at the ocean surface would also be reduced. However, our coupled model results show that the meridional gradient of surface density actually increases with increasing CO_2 concentration for warmer climates. This is reflected in the fact that the thermohaline circulation shown in Figure 13 does not show any substantial difference in intensity among the high-CO_2 climates. The explanation for this surprising behavior can be obtained from Figure 14*a*. At higher temperatures the coefficient of expansion of seawater is greatly increased. Therefore small increments of temperature at low latitudes cause the same change in density as much larger increments of temperature in a lower range at high latitudes. This effect compensates for polar amplification of the temperature response and maintains or slightly increases the total meridional density contrast at the ocean surface.

4.4. *Poleward Energy Transport*

In the preceding section it is shown that the meridional gradient of zonal mean surface air temperature reduces markedly with increasing CO_2 concentration of air. One of the important factors which control the meridional temperature gradient in the atmosphere and ocean is the poleward energy transport by the combined system. Therefore this section is devoted to the discussion of the poleward energy transport in the coupled model.

One can classify the total poleward energy transport into the atmospheric and oceanic components. The atmospheric component may be divided further into the transports of dry static energy ($C_pT + \phi$) and latent heat ($L \times r$). (Here C_p is the specific heat of air, T is temperature, ϕ is geopotential height, L is the latent heat of evaporation, and r is the mixing ratio of water vapor in air.) Figure 15 illustrates the latitudinal distribution of the poleward transport of total energy by both the atmosphere and the ocean of the model. In Figure 16 this total energy transport is broken down into the dry static energy, latent heat, and oceanic sensible heat components.

It is of particular interest that the total energy transport by the joint system (shown in Figure 15) is relatively insensitive to the general reduction of the meridional temperature gradient in the lower model troposphere as CO_2 concentration increases from the 1X to the 8X experiments. Although the poleward transport of dry static energy reduces with increasing CO_2 concentration in middle latitudes, that of latent heat increases markedly (as Figure 16 indicates) owing to the increase of moisture content of air [*Manabe and Wetherald*, 1980]. On the other hand, in low latitudes, the poleward transport of dry static energy increases with increasing CO_2 and counterbalances the increase in the equatorward transport of latent heat. This increase in the poleward transport of dry static energy is due to the intensification and the upward stretching of the Hadley cell described earlier. As was pointed out by *Held and Hoskins* [1985], the upward stretching of the Hadley cell contributes to the increase of the poleward transport of potential energy and accordingly that of dry static energy. The increase in the equatorward transport of latent energy from the 1X experiment to the 8X experiment is attributable not only to the intensification of the Hadley cell but also to the increase in the moisture content of air accompanied by the CO_2-induced warming. In summary, the magnitude of the total poleward energy transport at all latitudes is very similar among the 1X, 2X, 4X, and 8X experiments because of the compensation between the changes in the transports of latent energy and those of dry static energy.

On the other hand, the total poleward transport by the joint

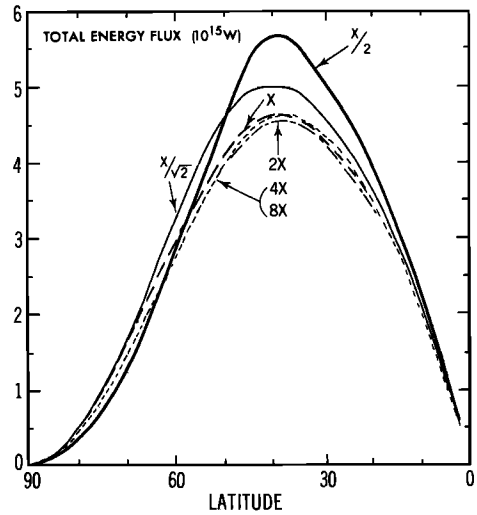

Fig. 15. Poleward transport of total energy by the joint ocean-atmosphere system of the model in the six experiments. Units are in 10^{15} W. Three sector oceans and three sector atmospheres, which cover an entire hemisphere, are involved in this transport.

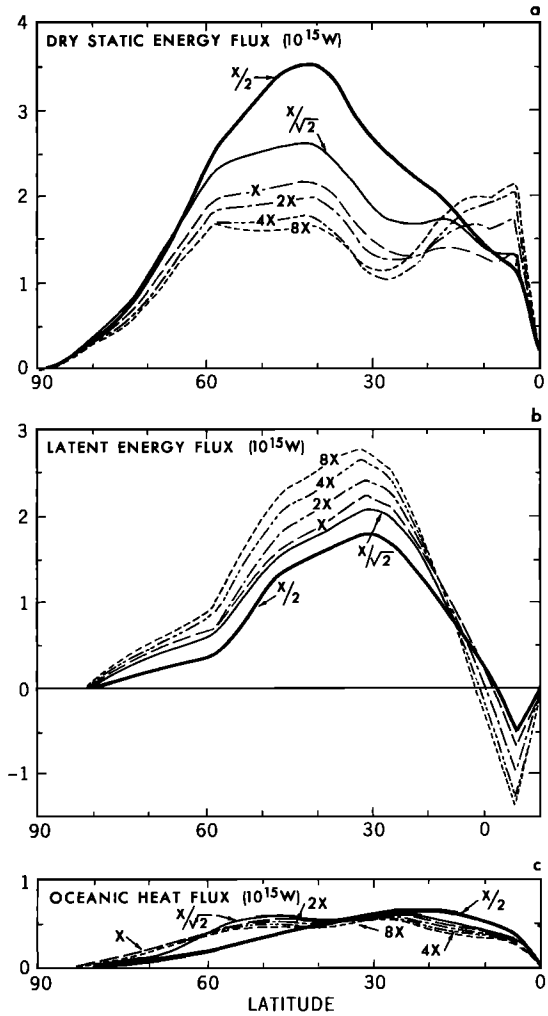

Fig. 16. Poleward transport of (*a*) dry static energy, (*b*) latent energy in the model atmosphere, and (*c*) oceanic heat transport in the six experiments. Units are in 10^{15} W. Note that three sector oceans and three sector atmospheres, which cover an entire hemisphere, are involved in these transports.

system in the X/2 and $X/\sqrt{2}$ experiments is significantly larger than the transport in the other experiments, with the exception of high latitudes. As Figure 16 indicates, the various components of transport in these two experiments do not compensate for each other as they did in other experiments.

Although the poleward heat transport by ocean currents appears relatively small, it reduces significantly in high latitudes from the $X/\sqrt{2}$ experiment to the X/2 experiments and exerts a major influence upon the surface air temperature. Also, some reduction occurs from the 1X to the $X/\sqrt{2}$ experiments poleward of 60° latitude. These reductions of poleward oceanic heat transport result from the weakening and equatorward contraction of the thermohaline circulation cell discussed in section 4.3. It is accompanied by a marked reduction of the upward heat supply from the ocean surface and the cooling of the surface layer of the atmosphere in the ice-covered region, where the air-water exchange of heat is reduced by the intervening sea ice. It also results in the increase of upward heat supply along the outer periphery of the sea ice margin. (See Figure 17). The weakening of thermohaline circulation by sea ice further enhances the reduction of surface air temperature caused by the effective reflection of solar radiation by sea ice. Since the surface layer of the model atmosphere over the ice-covered region has a very stable stratification, the cooling is limited to the lowest layer of the atmosphere. On the other hand, the warming due to the increase in the convergence of poleward oceanic heat transport along the periphery of sea ice is relatively small because the heating spreads over a thicker layer of the model atmosphere. The large cooling of surface air over sea ice–covered regions contributes to the equatorward expansion of sea ice and the drastic reduction of surface air temperature from the $X/\sqrt{2}$ experiment to the X/2 experiments. Thus the sensitivity of the present coupled model with low atmospheric concentration of CO_2 is much larger than the sensitivity of the model atmosphere coupled to a stagnant ocean mixed layer with comparable surface air temperature as discussed in the appendix. The marked change in oceanic transport is responsible for this difference.

The enhancement of the lower tropospheric cooling in high latitudes through the interaction between sea ice and thermohaline circulation is an intriguing process. As is discussed in the concluding section, a similar weakening of thermohaline circulation may have occurred in the North Atlantic during the last glacial maximum. However, it is likely that the present model with three sector oceans resembling the North Atlantic may exaggerate the influence of this positive feedback process.

4.5. *Hydrology*

The relationship between the intensity of the hydrologic cycle and the CO_2 concentration in the model atmosphere may be inferred from Table 3, which tabulates the area mean rates of precipitation and runoff from all six experiments. According to this table the rate of precipitation averaged over the entire computational domain increases significantly with increasing CO_2 concentration. Similar changes also occur in the area mean rate of evaporation, because in a steady state, the area mean rates of precipitation and evaporation are equal to one another. When one compares the area mean rates of precipitation with the area mean temperature in Table 3, one notes that, in general, the warmer the model climate, the more intense the hydrologic cycle. As a matter of fact, there exists an almost linear relationship between the two quantities. The physical mechanisms which are responsible for the CO_2-induced intensification of the hydrologic cycle were discussed by *Wetherald and Manabe* [1975] and *Manabe and Wetherald* [1975], based upon the analysis of the climate sensitivity experiments which they conducted. As they explained, this intensification results partly from the increase of downward flux of terrestrial radiation at the earth's surface, which is due to the increase in CO_2 concentration and the accompaning increase of the mixing ratio of water vapor in air. In order to maintain the surface heat balance, this increased downward radiative flux necessitates the enhanced removal of energy from the surface through evaporation and the boundary layer flux of sensible heat. Furthermore, the CO_2-induced surface warming raises the saturation vapor pressure at the earth's surface and thereby increases the fraction of energy removed through evaporation (rather than sensible heat flux). This explains why the area mean rate of evaporation (and accordingly that of precipitation) increases so sharply with increasing CO_2 concentration in the model atmosphere.

The intensification of the hydrologic cycle discussed in the preceding paragraph produces a change in the rate of runoff from the continent of the model. Table 3 indicates that the area mean rate of runoff over the continents increases mark-

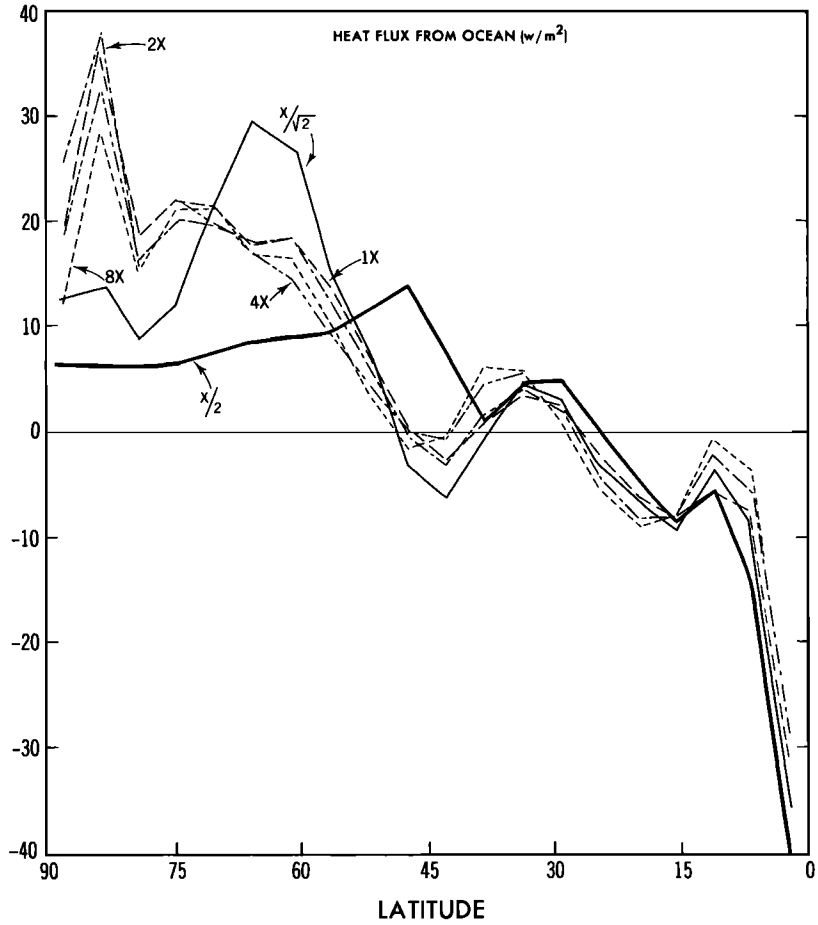

Fig. 17. The latitudinal profiles of the upward heat flux at the ocean surface in units of watts per square meter obtained from the six experiments.

edly from the X/2 experiment to the 8X experiment. As was pointed out, for example, by *Berner et al.* [1983], large runoff can enhance weathering in a CO_2-rich world.

The latitudinal distributions of zonal mean rates of precipitation and evaporation from five experiments are illustrated in Figure 18. According to this figure the rate of evaporation increases at all latitudes as the atmospheric CO_2 concentration changes from the X/2 experiment to the 8X experiment. On the other hand, the CO_2-induced change in precipitation rate depends very much upon latitude. For example, the precipitation rate is nearly constant in the subtropical belt of minimum precipitation, whereas it increases markedly in middle and high latitudes and in the tropics in response to the CO_2 change. One can understand these changes in precipitation rate by referring to the CO_2-induced change in the poleward transport of moisture discussed in section 4.4. The large increase in middle and high latitudes is attributable to the increase in the poleward transport of moisture by large-scale eddies from the subtropics to higher latitudes discussed in section 4.4. On the other hand, the tropical increase in the

TABLE 3. Area Mean Rates of Precipitation and Runoff in Units of Centimeters Per Day From All Six Experiments

Experiment	Precipitation (or Evaporation)		Runoff		Area Mean Surface Air Temperature, °C
	Area Mean Rate, cm/d	Relative Magnitude	Area Mean Rate, cm/d	Relative Magnitude	
X/2	0.156	0.75	0.020	0.54	2.6
$X/\sqrt{2}$	0.190	0.91	0.030	0.81	10.3
1X	0.208	1.00	0.037	1.00	14.4
2X	0.224	1.08	0.041	1.11	17.6
4X	0.238	1.14	0.047	1.27	19.8
8X	0.247	1.19	0.049	1.32	21.7

Precipitation rate is an average over the entire computational domain, and runoff rate represents an average over the continent. In the columns identified as relative magnitude, these rates are normalized by the rates from the 1X experiment. The last column contains the area mean values of surface air temperature in degrees Celsius.

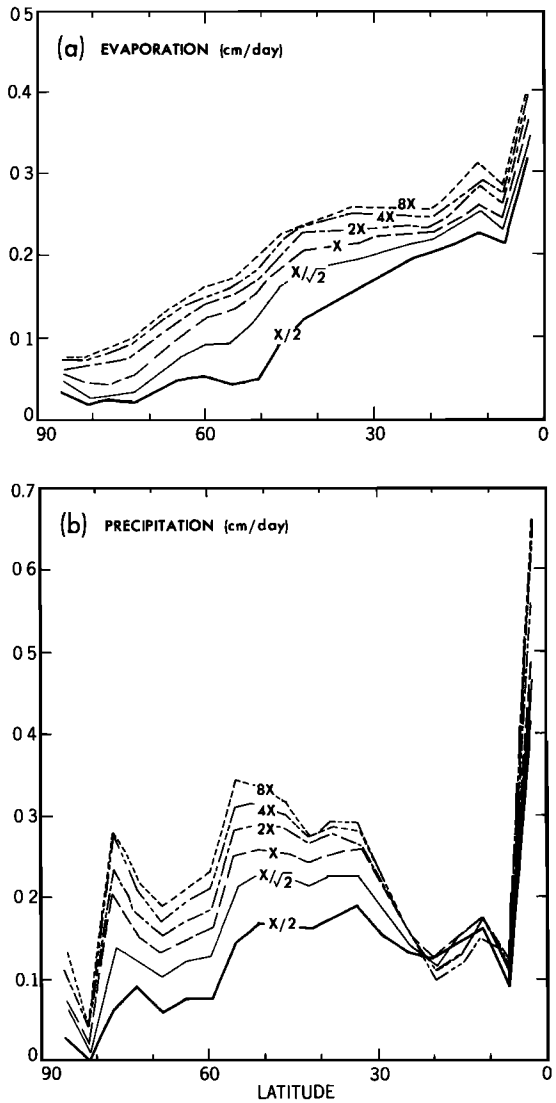

Fig. 18. Latitudinal distribution of zonal mean rates (in centimeters per day) of (*a*) evaporation and (*b*) precipitation from the X/2, X/$\sqrt{2}$, 1X, 2X, 4X, and 8X experiments.

precipitation rate is attributable to the enhanced equatorial transport of moisture by the Hadley cell. This enhancement results from (1) the intensification of the Hadley cell and (2) the increase in the moisture content of air. Because of the increased export of moisture towards the equator and high latitudes, the rate of precipitation in the model subtropics hardly changes from the 1X experiment to the 8X experiments despite the increase in evaporation rate.

According to Figure 19, which illustrates the latitudinal profiles of the difference between the zonal mean rate of precipitation and that of evaporation, the earth's surface of the model gains moisture in the tropics and high latitudes and loses it in the subtropics. Because of the CO_2-induced change in the atmospheric transport of moisture discussed in the preceding paragraph, the rate of net gain and loss of moisture at the surface increases with increasing CO_2. Thus the range of latitudinal salinity variation at the ocean surface also increases with increasing CO_2, as is illustrated by Figure 14.

It is of interest that in Figure 19, the subtropical belt of the maximum moisture depletion at the earth's surface is located at about the same latitude for all CO_2 experiments. Some evidence that this result is consistent with geological evidence is provided by *Gordon* [1975] in a study of Phanerozoic evaporites. It is known that evaporites tend to be deposited in the subtropical zones of each hemisphere, where evaporation substantially exceeds precipitation. Gordon summarized the latitude of evaporite deposits over the entire globe, correcting for the plate movements. The results are shown in Figure 20. The data indicate that evaporites occur in essentially the same latitudes as they do today as far back as the lower Paleozoic. In summary, the location of evaporite deposits is consistent with the constancy of the subtropical zone of maximum surface moisture depletion in the experiments conducted in this study.

Similarly, one can detect very little difference in the latitudes of the subtropical high and the jet stream among the results from the X/$\sqrt{2}$, 1X, 2X, 4X, and 8X experiments as noted earlier. The invariability of the latitude of the subtropical high appears to be consistent with the constancy of the subtropical belt of maximum surface moisture depletion. The constancy of the latitude of the evaporite zone described above encourages one to speculate that the atmosphere of the warm Mesozoic era possessed a structure similar to the model atmosphere emerging from a high-CO_2 experiment.

5. Concluding Remarks

As was pointed out in the report from the *National Academy of Sciences* [1982], a large quantitative uncertainty remains in estimates of climate sensitivity to a change of CO_2 concentration in the atmosphere. However, many qualitative features of CO_2-induced change of climate obtained in this study are less controversial and have been shown in CO_2 climate sensitivity studies previously published. Some of these features include polar amplification of surface temperature change and intensification of the hydrologic cycle. A new feature of the present study is the consideration of a much wider range of atmospheric CO_2 concentration and the inclusion of an active ocean circulation in the climate model.

If one compares the climate equilibria which are obtained for the normal CO_2 concentration and 8 times the normal CO_2 concentration of air, one notes that the CO_2-induced increase of surface air temperature is particularly large in high latitudes. Thus the meridional gradient of surface air temper-

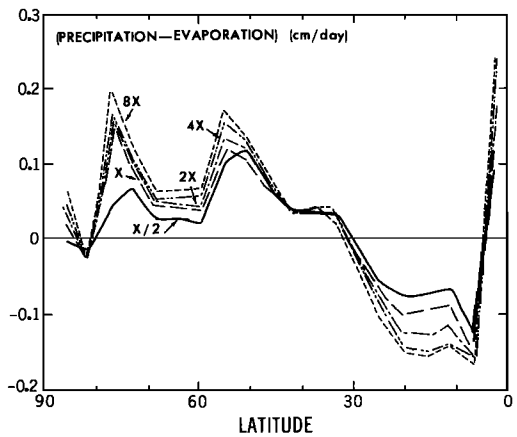

Fig. 19. Latitudinal distributions of the difference between the rate of precipitation and that of evaporation from the X/2, 1X, 2X, 4X, and 8X experiments. Units are in centimeters per day.

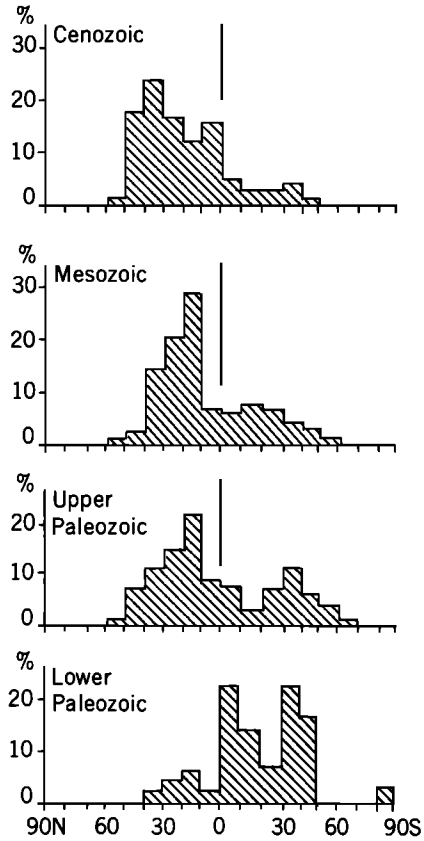

Fig. 20. Distribution of ancient evaporite by latitude compiled by *Gordon* [1975]. The evaporites are plotted by era grouping with reference to paleolatitude.

ature is reduced. On the other hand, the meridional gradient of temperature in the upper model troposphere increased with increasing atmospheric CO_2 concentration. Since these changes of meridional temperature gradient in the upper and lower model troposphere have opposite influences upon the vertical shear of zonal wind, the intensity of the jet stream in the upper model troposphere is hardly affected by the eightfold increase in the concentration of atmospheric CO_2. Furthermore, there is almost no shift in the latitudinal placement of the jet stream.

The polar amplification of the CO_2-induced temperature change also occurs in the upper layer of the model ocean, though the increase of sea surface temperature in high latitudes is somewhat smaller than that of surface air temperature because of the constraint imposed by the freezing of seawater. Since most of the deep water in the model ocean is formed at the surface in high latitudes, the deep ocean is very sensitive to this polar amplification. Therefore the change in deep water temperature of the model should not be taken as representative of the globally averaged change of surface temperature. The distribution of the CO_2-induced change of temperature in the model ocean is qualitatively similar to the Tertiary change of ocean temperature inferred from the oxygen 18 analysis of planktonic and benthic foraminifera [*Savin*, 1977]. At high latitudes of the model, surface and deep water temperature respond to a change of atmospheric CO_2 concentration in the same way, while at low latitudes the response of sea surface temperature is much less than that of deep water. Since the present model does not include a shallow epeiric sea, it does not allow a real test of *Chamberlin*'s [1906] hypothesis that deep waters of the Cretaceous and early Tertiary were formed in the shallow sea at low latitudes. Nevertheless, the CO_2 hypothesis of warm climate provides a plausible alternative to Chamberlin's mechanism for the formation of warm deep water. The results from the present model are consistent with Emiliani's suggestion that deep water continues to be formed at high latitudes in climates which are much warmer than today's [*Emiliani*, 1954].

An unexpected result involves the intensity of thermohaline circulation. Intuition would suggest that the meridional density gradient at the ocean surface would decrease in warmer climates because of the reduction in meridional temperature gradient. The results from the present study indicate that the meridional density gradient at the ocean surface actually increases slightly with increasing atmospheric CO_2. This surprising result is traced to the fact that the thermal expansion coefficient of seawater increases with temperature. Thus for warmer climates, the smaller meridional temperature gradient does not necessarily imply a smaller meridional density gradient. Owing to this effect the intensity of thermohaline circulation in the model ocean is nearly constant over a wide range of warm climates. A dramatic change in the thermohaline circulation occurs when the atmospheric CO_2 is reduced from the normal to one-half the normal concentration. In the reduced CO_2 case the sea surface temperature is held at the freezing point from the pole down to 45° latitude because of the formation of sea ice. Thus the thermohaline circulation is relatively weak and is largely confined to the region between the ice edge and the equator.

Owing to the weakening and the equatorward contraction of the thermohaline cell discussed above, the poleward heat transport by ocean currents decreases significantly in high latitudes in response to the reduction of the atmospheric CO_2 from normal to half normal values. This implies a reduction of upward oceanic heat flux over the region covered by sea ice. Such a reduction causes an intense cooling limited to the very stable surface layer of the atmosphere, inducing the further extension of sea ice with high surface albedo. This interaction between thermohaline circulation and sea ice described above appears to be responsible for the extremely large cooling of surface air temperature in high latitudes when the CO_2 concentration of the model atmosphere is reduced substantially from the normal value. Since the present model has three idealized sector oceans extending all the way to the pole, it is likely that the model exaggerates the magnitude of surface air temperature reduction due to the weakening of thermohaline circulation. Thus one should not take too literally the large difference in surface air temperature between the model atmospheres with the normal concentration and half the normal concentration of CO_2. Nevertheless, the present study identifies a positive feedback process which may have played an important role in inducing the cold climate of an ice age. Evidence from faunal, chemical, and isotopic studies of deep-sea sediments suggests that the production of deep water was greatly reduced and the coverage of sea ice was very extensive in the North Atlantic during the last glacial maximum. (See, for example, *Broecker et al.* [1985] and *Boyle and Keigwin*, 1982].) These results suggest that the positive feedback process, which involves the interaction between sea ice and thermohaline circulation, operated in the North Atlantic and helped to induce low surface air temperature in high latitudes during the last ice age. This process, together with the albedo feedback process of snow over continents, explains why the

very cold climate with low atmospheric CO_2 is much more sensitive than the warm climate with high CO_2.

As the CO_2 concentration increases from the normal to 8 times the normal value, the global mean rate of precipitation increases by about 19% and that of global runoff increases by as much as 32%. The increase in runoff is particularly marked at high latitudes because of the greatly enhanced poleward transport of water vapor in warm climates. The latitude of the arid zone and the high-surface-pressure belt in the subtropics is insensitive to an eightfold increase in CO_2 concentration, which appears to be consistent with geological evidence from evaporite deposits.

While the CO_2-induced change of the model climate generally resembles the Tertiary change of climate inferred from stable isotope and other geological data, there is one notable exception. This involves the estimate of paleotemperature of surface water in the tropics. The model indicates an increase of about 5°C for an eightfold increase of atmospheric CO_2, while sea surface temperature inferred from the isotopic analysis of planktonic foraminifera [*Savin et al.*, 1975] indicates no systematic trend during the Tertiary.

The above discussion would not be complete without several important caveats concerning the model. One of these caveats involves the absence of the cloud feedback process in the present model. The recent study of CO_2 climate sensitivity by *Hansen et al.* [1984] suggests that the CO_2-induced change of cloud cover can enhance the sensitivity of climate. On the other hand, the study of *Somerville and Remer* [1984] raised the possibility that the change in the liquid water content, and accordingly the albedo of cloud cover due to the CO_2-induced warming of air, reduces the sensitivity of climate. In view of uncertainties on the role of the cloud feedback process in determining the sensitivity of climate, it was decided not to attempt a prediction of the distribution of cloud cover in the present model. If and when this feedback process is better understood, the quantitative aspect of the present results may have to be adjusted accordingly.

The interpretation of the results from the model also depends on the implicit assumption that seasonal effects and the details of the continent-ocean distribution are secondary factors relative to the substantial change in the CO_2 concentration of the atmosphere. However, these assumptions would not be accepted by many paleoclimatologists and remain to be tested.

Recently, *Manabe and Broccoli* [1985] attempted to simulate the climate of the last glacial maximum by use of a general circulation model of the atmosphere coupled with a static model of a mixed layer ocean. Their model has a realistic geography and seasonal variation of insolation. Despite the neglect of the effect of lateral oceanic heat transport, the model simulates reasonably well the cold sea surface temperature of the last glacial maximum as reconstructed by the *CLIMAP Project Members* [1981]. Their results suggest that for the simulation of a cold ice age climate, it may not be necessary to have the enhancement of climate sensitivity by thermohaline circulation described in this study. However, one should recall that Manabe and Broccoli prescribed the continental ice sheets of the last glacial maximum and low atmospheric CO_2 concentration (i.e., 200 ppm by volume) in their simulation experiment. In order to explain the transformation of both climate and continental ice sheets all the way from the interglacial to glacial epochs, it may well be necessary to take this positive feedback process into account.

One should also note that the present model completely bypasses the interaction of climate and the carbon cycle itself. Evidence from the Pleistocene suggests that the carbon cycle may provide a positive climate feedback which could greatly amplify a climate change induced in some other way rather than being a primary cause. Further research may show that the same is true for earlier geologic periods. A final caveat concerns the ocean component of the climate model for this study. Because of the low spatial resolution of the finite difference grid and the attendant viscosity, the model has a very sluggish ocean circulation and has unrealistically small poleward heat transport by ocean currents in low latitudes [*Spelman and Manabe*, 1984]. While the model ocean plays a very significant role in increasing climate sensitivity in the cold climate regimes, the weak thermohaline regime may prevent the model ocean from playing as significant a role in warmer regimes. For this reason it would be desirable to repeat the numerical experiments using an ocean model with higher computational resolution.

APPENDIX: OCEAN CURRENTS AND THE ENHANCEMENT OF CLIMATIC SENSITIVITY

To evaluate how the change in ocean circulation affects the sensitivity of climate, an equilibrium response of the present model (MI) to an increase of atmospheric CO_2 is compared with a response of another model (MII) without the effect of oceanic heat transport. This MII model is identical to the MI model except that its oceanic component consists of a stagnant, vertically isothermal, and 50-m-thick mixed layer rather than a general circulation model.

As was noted, for example, by *Spelman and Manabe* [1984], surface air temperature in high latitudes strongly influences the sensitivity of a model climate. This is because it essentially determines the equatorward margins of snow and sea ice which control the albedo feedback process. In order to estimate the influence of ocean currents upon the sensitivity of climate, it is therefore desirable to compare the sensitivity of the MI and MII models, which have approximately the same surface air temperature in high latitudes and accordingly albedo feedback processes of comparable effectiveness. Such a comparison may be made by use of Figure A1. This figure illustrates the latitudinal profiles of zonal mean surface air temperature from two series of the CO_2 experiment by use of the MI and MII models. When one compares the difference in surface air temperature of the MI model between the X/2 and $X/\sqrt{2}$ experiments with the corresponding difference in the MII model between the 1X and 2X experiments, one notes that the former is almost as large as the latter. Since the warming effect of CO_2 is approximately proportional to the increase in the logarithm of atmospheric CO_2, this implies that the sensitivity of the MI model climate from the X/2 experiment is almost twice as large as that of the MII model climate from the 1X experiment, which has a similar surface air temperature in high latitudes. As is discussed in section 4, this large sensitivity of the MI model with low CO_2 concentration is attributable to the interaction between the sea ice and thermohaline circulation.

To compare the sensitivity of the MI and MII models in a simpler manner, the area mean values of surface air temperature from the two series of CO_2 experiments obtained from the two models are plotted in Figure A2. This figure indicates that the area mean 8X surface air temperature from the MII model is not very different from the corresponding temperature from the MI model. However, as the atmospheric concentration of carbon dioxide reduces from the 4X experiment

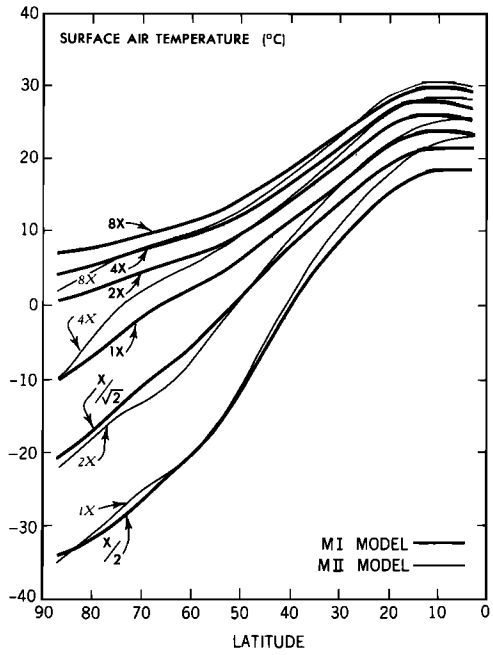

Fig. A1. The latitudinal profiles of zonal mean surface air temperature in units of degrees Celsius. Thick solid lines indicate profiles from the MI model. Thin solid lines indicate profiles from the MII model. The oceanic component of the MI model is a general circulation model. On the other hand, that of the MII model is a mixed layer ocean model.

to the 1X experiment, the area mean surface air temperature of the MII model reduces much more sharply than that of the MI model. Because of the lack of poleward heat transport by ocean currents and the dominating influence of the albedo feedback process involving snow and sea ice, the MII model has a lower surface air temperature in high latitudes and is much more sensitive than the MI model in these experiments, as was noted in the study of *Spelman and Manabe* [1984].

The situation reverses as the concentration of carbon dioxide reduces further from the 1X to the X/2 experiment. According to Figure A2, the area mean surface air temperature of the MI model reduces sharply with decreasing CO_2 concentration from the $X/\sqrt{2}$ to X/2 experiments. This reduction is much steeper than the corresponding reduction of the MII model with comparable area mean surface air temperature. As is discussed in section 4, this steep reduction from the MI model is attributable to the enhancement of the sea ice albedo feedback process caused by the change in the intensity of thermohaline circulation.

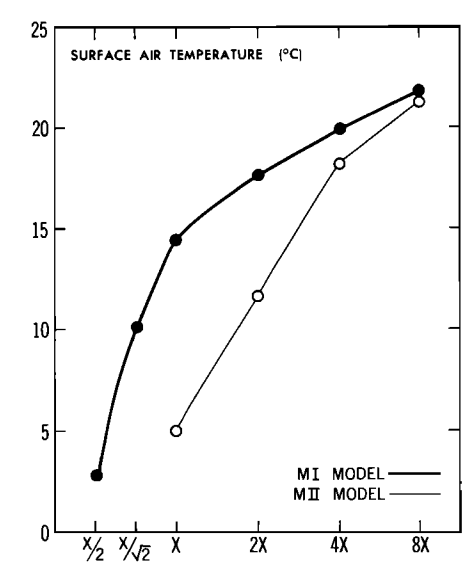

Fig. A2. The area mean surface air temperature from two series of the CO_2 experiments. The thick solid line denotes the MI model. The thin solid line denotes the MII model.

Acknowledgments. The authors acknowledge the major effort of M. J. Spelman, who constructed the massive computer program of the coupled ocean-atmosphere model and conducted the numerical experiments described in this study. He played a key role in the successful completion of this project. I. M. Held gave much valuable advice throughout the course of this study. S. Fels and D. Schwarzkopf kindly evaluated the influence of the 10-μm CO_2 band upon the radiative, convective equilibrium of the atmosphere. The authors wish to thank GFDL staff members P. Tunison and J. Conners for the preparation of the figures and J. Kennedy for the efficient typing of the manuscript.

REFERENCES

Barron, E. J., and W. M. Washington, The role of geographic variables in explaining paleoclimates: Results from Cretaceous climate model sensitivity studies, *J. Geophys. Res.*, *89*, (D1), 1267–1279, 1984.

Berner, R. A., A. C. Lasaga, and R. M. Garrels, The carbonate-silicate geochemical cycle and its effect on atmospheric carbon dioxide over the past 100 million years, *Am. J. Sci.*, *283*, 641–683, 1983.

Boyle, E. A., and L. D. Keigwin, Deep circulation of the North Atlantic over the last 200,000 years: Geochemical evidence, *Science*, *218*, 784–787, 1982.

Broecker, W. S., D. M. Peteet, and D. Rind, Does the ocean-atmosphere system have more than one stable mode of operation?, *Nature*, *315*, 21–26, 1985.

Bryan, F., Maintenance and variability of the thermohaline circulation, Ph.D. thesis, Princeton Univ., Princeton, N. J., 1985.

Bryan, K., and L. J. Lewis, A water mass model of the world ocean, *J. Geophys. Res.*, *84*(C5), 2503–2517, 1979.

Bryan, K., Accelerating the convergence to equilibrium of ocean-climate models, *J. Phys. Oceanogr.*, *14*(4), 666–673, 1984.

Bryan, K., and M. J. Spelman, The ocean's response to a CO_2-induced warming, *J. Geophys. Res.*, this issue.

Bryan, K., S. Manabe, and R. C. Pacanowski, A global ocean-atmosphere climate model, II, The oceanic circulation, *J. Phys. Oceanogr.*, *5*, 30–46, 1975.

Bryan, K., F. G. Komro, S. Manabe, and M. J. Spelman, Transient climate response to increasing atmospheric carbon dioxide, *Science*, *215*, 56–58, 1982.

Bryden, H. L., and M. M. Hall, Heat transport by ocean currents across 25°N latitude in the Atlantic, *Science*, *207*, 884–886, 1980.

Budyko, M. I., and A. B. Ronov, Chemical evolution of the atmosphere in the Phanerozoic, *Geochemistry*, *5*, 643–653, 1979.

Budyko, M. I., and M. A. Efimova, The influence of carbon dioxide on climate (in Russian), *Meteorol. Gidrol.*, No. 2, 5–17, 1981.

Chamberlin, T. C., An attempt to frame a working hypothesis of the cause of glacial periods on an atmospheric basis, *J. Geol.*, *7*, 545–584, 1899.

Chamberlin, T. C., On a possible reversal of deep sea circulation and its influence on geologic climates, *J. Geol.*, *14*, 363–373, 1906.

CLIMAP Project Members, Seasonal reconstructions of the earth's surface at the last glacial maximum, *Geol. Soc. Am. Map. Chart. Ser.*, *MC-36*, 1981.

Crutcher, H. L., and J. M. Meserve, Selected level heights, temperatures, and dew points for the northern hemisphere, *Rep. NAVAIR 50-IC-52*, U.S. Nav. Weather Serv., Washington, D. C., 1970.

Emiliani, C., Temperature of Pacific bottom waters, and polar superficial waters during the Tertiary, *Science*, *119*, 853–855, 1954.

Gordon, W. A., Distribution by latitude of Phanerozoic evaporite deposit, *J. Geol.*, *83*, 671–684, 1975.

Gordon, C. T., and W. Stern, A description of the GFDL global spectral model, *Mon. Weather Rev.*, *110*, 625–644, 1982.

Hansen, J. E., A. Lacis, D. Rind, and G. Russell, Climate sensitivity:

Analysis of feedback mechanisms, in *Climate Processes and Climate Sensitivity, Maurice Ewing Ser.*, vol. 5 edited by J. E. Hansen and T. Takahashi, pp. 130–163, AGU, Washington, D. C., 1984.

Held, I. M., The tropospheric lapse rate and climate sensitivity: Experiments with a two-level atmospheric model, *J. Atmos. Sci., 35*, 2083–2098, 1978.

Held, I. M., and B. J. Hoskins, Large-scale eddies and the general circulation of the atmosphere, *Adv. Geophys., 28A*, 3–31, 1985.

Kondratyev, K. Ya., Radiation processes in the atmosphere, *WMO Publ., 309*, 1–10, 1972.

London, J., A study of the atmospheric heat balance, final report, contract AF19(122)-65, 99 pp., Res. Div., Coll. of Eng., N. Y. Univ., N. Y., 1956.

Manabe, S., Climate and ocean circulation, I, The atmospheric circulation and hydrology of earth's surface, *Mon. Weather Rev., 97*, 739–774, 1969.

Manabe, S., CO_2 and climatic change, *Adv. Geophys., 25*, 39–82, 1983.

Manabe, S., and A. J. Broccoli, A comparison of climate sensitivity with data from the last glacial maximum, *J. Atmos. Sci.*, in press, 1985.

Manabe, S., and K. Bryan, Climate calculations with a combined ocean-atmosphere model, *J. Atmos. Sci., 26*, 786–789, 1969.

Manabe, S., and R. T. Wetherald, The effect of doubling the CO_2-concentration on the climate of a general circulation model, *J. Atmos. Sci., 32*, 3–15, 1975.

Manabe, S., and R. T. Wetherald, On the distribution of climate change resulting from an increase of CO_2-content of the atmosphere, *J. Atmos. Sci., 37*, 99–118, 1980.

Manabe, S., J. Smagorinsky, and R. F. Strickler, Simulated climatology of a general circulation model with a hydrologic cycle, *Mon. Weather Rev., 93*, 769–798, 1965.

Manabe, S., K. Bryan, and M. J. Spelman, A global ocean-atmosphere climate model, I, The atmospheric circulation, *J. Phys. Oceanogr., 5*, 3–29, 1975.

National Academy of Sciences, *Carbon Dioxide and Climate: A Second Assessment*, National Academy Press, Washington, D. C., 1982.

Neftel, A., H. Oeschger, B. Stauffer, and R. Zumbrunn, Ice core sample measurements give atmospheric CO_2-content during the past 40,000 yr., *Nature, 295*, 220–222, 1982.

Oort, A. H., and E. M. Rasmusson, Atmospheric circulation statistics, *NOAA Prof. Pap., 5*, 1–323, 1971.

Orszag, S. A., Transform method for calculation of vector coupled sums: Application to the spectral form of the vorticity equation, *J. Atmos. Sci., 27*, 890–895, 1970.

Roemmich, D., Estimation of meridional heat flux in the North Atlantic by inverse method, *J. Phys. Oceanogr., 10*, 1972–1983, 1980.

Savin, S. M., The history of the earth's surface temperature during the past 100 million years, *Annu. Rev. Earth Planet. Sci., 5*, 319–355, 1977.

Savin, S. M., R. G. Douglas, and F. G. Stehli, Tertiary marine paleotemperatures, *Geol. Soc. Am. Bull., 86*, 1499–1510, 1975.

Shackleton, N. J., and J. P. Kennett, Paleotemperature history of the Cenozoic and the initiation of Antarctic glaciation: oxygen and carbon isotope analysis in DSDP sites 277, 279, and 281, *Init. Rep. Deep Sea Drill. Proj., 29*, 743–755, 1975.

Somerville, R. C. J., and L. A. Remer, Cloud optical thickness feedbacks and the CO_2 climate problem, *J. Geophys. Res., 89*(D6), 9668–9672, 1984.

Spelman, M. J., and S. Manabe, Influence of oceanic heat transport upon the sensitivity of a model climate, *J. Geophys. Res., 89*(C1), 571–586, 1984.

U.S. Navy Hydrographic Office, World atlas of sea surface temperature, *Publ. 225*, Washington, D. C., 1964.

Wetherald, R. T., and S. Manabe, The effect of changing the solar constant on the climate of a general circulation model, *J. Atmos. Sci., 32*, 2044–2059, 1975.

K. Bryan, Jr., and S. Manabe, Geophysical Fluid Dynamics Laboratory/NOAA, Princeton University, P. O. Box 308, Princeton, NJ 08542.

(Received May 6, 1985;
accepted June 20, 1985.)